Simplified Coherent Receiver for Analogue Radio Transmission over High Optical Budgets

Dinka Milovančev, *Member, IEEE,* Nemanja Vokić, *Member, IEEE,* Fotini Karinou, *Member, IEEE,* and Bernhard Schrenk, *Member, IEEE*

***Abstract*— The bandwidth and latency demands driven by 5G wireless networks are putting a focus on analog radio-over-fiber techniques as a promising candidate for broadband optical fronthauling. In contrast to intensity modulation / direct detection systems, as they are commonly adopted for mobile fronthaul links due to their simplicity, we are exploring a migration option towards coherent radio-over-fiber transmission. A simplified coherent homodyne receiver based on an electro-absorption modulated laser is co-integrated at the die-level with a transimpedance amplifier and evaluated for analogue coherent radio-over-fiber transmission. This low-complexity homodyne receiver can unlock channel selectivity and high receiver sensitivity inherent to coherent detection, but without the need for digital signal processing. We will demonstrate a sensitivity that allows for an optical budget of 42 dB, and thus eases the fixed-mobile convergence in power-splitting fiber plants. We further show filterless radio signal reception in presence of modulated adjacent channels. Signal integrity is confirmed through transmission of orthogonally frequency multiplexed radio signals with 16-point quadrature amplitude modulated formats, with an error vector magnitude below the corresponding antenna limit.**

***Index Terms*— Optical communication terminals, Optical signal detection, Homodyne detection, 5G, Mobile fronthaul**

I. Introduction

RADIO-OVER-FIBER (RoF) systems have evolved during the past decades, shifting the focus from optical fiber backhaul schemes that connect a central office (CO) and base stations with field-deployed signal processing to optical fiber fronthaul applications, covering baseband units (BBU) with processing capabilities and remote radio heads (RRH). The optical fronthaul was developed within the 4G wireless standard by separating the BBUs from the antennas, previously situated with the antenna towers. Instead, the BBUs were then connected via optical fibers to the RRHs as a first step toward centralized/cloud-computing based radio access network (C-RAN) architectures. More recently, the development of a mobile fronthaul is driven by 5G specific demand profiles [1], such as bandwidth-hungry user applications in the context of enhanced mobile broadband (high-definition streaming, video and web conferencing, cloud storage), augmented and virtual reality applications, and addressing the smart cities and the Internet-of-Things paradigms. The scarcity of available RF spectrum is shifting the carrier frequencies toward the mm-wave spectrum [2], requiring architectural changes that come with ultra-densely packed cells in need of simplified RRHs, and having more efficient centralized signal processing and management with shared resources in terms of a remote BBU pool in the cloud and at the edge.

With the rising 5G demands, commonly adopted digital radio-over-fiber (D-RoF) does not always scale well. In D-RoF, the wireless data is digitized before being sent through optical fiber in compatibility with the Common Public Radio Interface (CPRI), but such a strategy is not very bandwidth-efficient since a high resolution is needed for the digitization, together with oversampling requirements. These yield a high CPRI rate, while the data rate available to the user is just a small fraction of the total CPRI rate.

In order to satisfy the rising bandwidth and latency requirements, there has been a growing interest in analog radio-over-fiber (A-RoF) approaches that are known to support high CPRI-equivalent data rates. The transmission of A-RoF offers a much better bandwidth utilization with a strong potential for simplified RRH equipment that is free of digital signal processing (DSP) resources. On the other hand, A-RoF comes with its own set of challenges such as fiber chromatic dispersion, the non-linearities due to opto-electric conversion and highly sensitive receivers to omit optical amplification. The most common way of A-RoF implementations is based on intensity modulation (IM) and direct detection (DD). IM/DD can meet the bandwidth requirements and uses simple transmitter and receiver components, thus offering low system complexity but at the expense of a poor receiver sensitivity. There are also microwave photonic approaches where radio up-conversion is facilitated by beating optical tones in order to accomplish mm-wave carriers with elevated frequencies such as 60 GHz [3].

The analogue transport of the radio signal at its target radio

This Manuscript received March 31, 2021. This work was supported in part by the European Research Council (ERC) under the European Union's Horizon 2020 research and innovation programme (grant agreement No 804769) and by the Austrian Research Promotion Agency FFG through the TRITON project (grant agreement No 858697).

D. Milovancev, N. Vokic and B. Schrenk are with the AIT Austrian Institute of Technology, Center for Digital Safety&Security, Giefinggasse 4, 1210 Vienna, Austria (phone: +43 50550-4131; fax: -4150; e-mail: bernhard.schrenk@ait.ac.at).

F. Karinou is with Microsoft Research Ltd, Cambridge, CB1 2FB, United Kingdom (e-mail: fotini.karinou@microsoft.com).

This article has been accepted for publication in IEEE/OSA Journal of Lightwave Technology. This is the author's version which has not been fully edited and content may change prior to final publication. Citation information: DOI 10.1109/JLT.2021.3085517

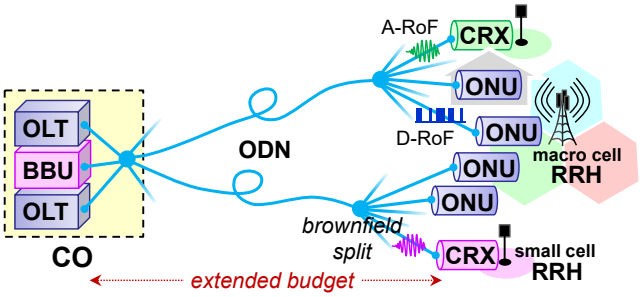

Fig. 1. Integration of radio-over-fiber transmission in wired brownfield ODN.

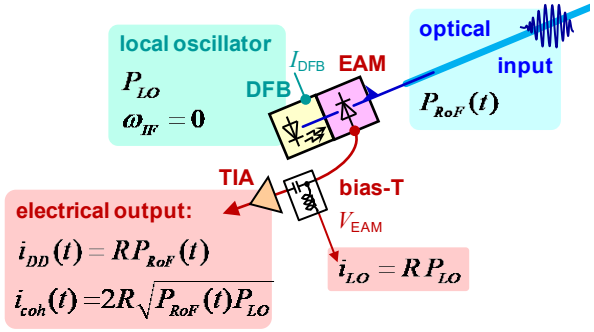

Fig. 2. EML+TIA receiver and resulting detection terms for coherent homodyne detection.

frequency (RF) carrier (A-RFoF) requires low phase noise and a precise setting for the optical emission frequency and, consequently, a high laser stability. Alternatively, an approach that is gaining attention is to transport the radio signal at intermediate frequency (IF) over the fiber (IFoF). Cost-effective mature opto-electronics with relaxed bandwidth requirements can be leveraged, with a complexity trade-off against RF componentry as needed for the up/down-conversion to the final carrier frequency. As a method of improving the performance of A-RoF systems, DSP resources are often used, either to improve linearity through digital predistortion techniques, or as a mean for frequency and phase offset compensation in case of coherent detection. This, however, stands in great contrast with the principal idea of radio-transparent antenna remoting through transmission of the native radio signal in the optical domain.

In this work, we are building on a simplified coherent receiver approach through homodyne detector based on an electro-absorption modulated laser (EML) serving as the receiving element. This approach was pioneered in our previous study [4], where DSP-free coherent reception has been demonstrated. Here, we are building on this groundwork by using die-level components that allow for a hybrid co-integration of the EML with a transimpedance amplifier (TIA), thus offering higher bandwidth, better sensitivity and compactness. To the best of the authors knowledge, this paper, which extends our initial analysis [5], is the first reported work of using an EML+TIA for coherent homodyne detection. Besides the expected advances in terms of sensitivity, the simplified EML+TIA receiver further allows for filterless channel selectivity, thus allowing to introduce wavelength division multiplexing (WDM) in brownfield-oriented power-splitting optical distribution networks (ODN) without additional expenditures. Towards this direction, we experimentally demonstrate the operation of the EML+TIA coherent receiver in a DSP-free 5-channel A-RoF downlink over 28.8 km of fiber, over an optical loss budget that would correspond to 1:128 splitting loss.

The paper is organized as follows. Section II sets the scene for RoF transmission under fixed-mobile convergence and highlights the state-of-the-art in the respective field. Section III introduces the concept of the coherent homodyne receiver. The experimental arrangement is presented in Section IV, followed by a characterization of the proposed receiver in Section V. The performance of A-RoF transmission is reported in Section VI. Finally, Section VII concludes the work and discusses further outlook.

II. Radio-over-Fiber Transmission

The increased demands of 5G and C-RAN based mobile fronthaul make A-RoF technology a focus of research as a solution for high CPRI-equivalent data demands, where RF data would otherwise have to be digitized before being transported over fiber. In [6], a total cost of ownership was considered by assessing both capital and operational expenditures for a 10-year period, considering A- and D-RoF options. In terms of cost optimization, the increase of bandwidth efficiency through carrier aggregation was highlighted for A-RoF, and very high operational expenditures are attributed to D-RoF. The cost efficiency of A-RoF links, therefore, gives another benefit compared to D-RoF.

The context of the mobile optical fronthaul addressed in this work is illustrated in Fig. 1, together with the proposed implementation of the EML-inspired low-complexity receiver in Fig. 2. It is envisioned that BBUs with narrowband processing capabilities for the wireless domain are connected to many simplified RRHs. The fiber-optic distribution from each BBU to the RRHs is accomplished at the ODN. The typical fiber length between BBU and RRH should be in the range of 20 km to ensure that the round-trip time for radio transport is just a fraction of the latency limit that is set by the end-user application. Using WDM, a BBU can be connected to a specific RRH in a virtual point-to-point link, but this would require WDM (de)multiplexers or additional installation of fibers, thus raising the capital expenditures. Moreover, the deployment over a brownfield ODN, which originates from wired optical access, should be compatible with splitter-based passive optical networks (Fig. 1). In such a case of fiber-wireless convergence, it is advantageous to avoid colored components at the ODN.

By adopting coherent optical detection, a channel selection can be performed in a filterless fashion, and thus without the use of an optical filter at the receiver or a WDM-specific architecture. Another important trait of an optical fronthaul link is its transparency to the radio layer, i.e., there is no need for DSP functions or high-speed analog-to-digital or digital-to-

TABLE I
RECENT DEMONSTRATIONS OF RADIO-OVER-FIBER TRANSMISSION SYSTEMS

Ref.	RoF method	Detection	TX	RX	Sensitivity	Center frequency / bandwidth / modulation format / data rate	Fiber reach	Complexity
this work	A-RoF	Homodyne coherent	DFB + I/Q modulator	EML+TIA	-36.1 dBm	RF: 3.5 GHz, BW = 125 MHz 16-QAM OFDM	28.8 km + split	very low
[7]	D-FDM RoF	IM/DD	ADC + 1.5 GHz DML	APD+DAC	-21 dBm	48× 20-MHz LTE 64-QAM OFDM	5 km	DSP for CDA
[8]	A-RFoF φ-UpC	Heterodyning 2 lasers	2-laser beating, DFB+IM and ECL	70 GHz PD	2.5 dBm	RF: 53 GHz, BW = 4.2 GHz 16-QAM to 64-QAM OFDM	15 km	DSP, narrow oBPF, stable LS
[9]	A-RoF IFoF	IM/DD	DML	6 GHz PIN	-6 dBm b2b	IF: 1.6–2.4 GHz f_C = 27–28.3 GHz	1 km	low
[10]	A-RoF IFoF	IM/DD	DFB + MZM	10 GHz APD	-	IF: 5 GHz, RF: 60 GHz, SDM, FDM BW = 950 MHz, 100 Mbaud QPSK	10 km	low
[11]	A-RFoF φ-UpC	Heterodyning	integrated laser, 90° hybrid, IQ modulator	70 GHz PIN + RF amplifier	1 dBm	RF: 60 GHz, UF-OFDM, 64QAM 0.89 Gb/s, 148.5 MHz, oSSB	25 km	oBPF
[12]	A-RFoF φ-UpC	Heterodyning 2-tone beating	2×MZM (oCS + SSB/DSB)	PIN Rx, eBPF	2-5 dBm	RF: 27 GHz, beating 2 tones	10 km	Stable LS, oBPF
[13]	A-RFoF	Heterodyning 2-tone beating	ECL + 2×MZM + WSS	40 GHz PD	3.5 dBm	RF: 28 GHz, 4-band M OFDM, CA, oCS, 1.2 – 4.8 Gbit/s BW: 491.5 MHz – 1.96 GHz	10 km	DSP, ECL, WSS
[14]	DSP-assisted A-RFoF	IM/DD	LS+MZM	10 GHz PIN	-	IF 5 GHz, RF 60 GHz, SCM UL: 1 Gb/s QPSK, DL: 12 Gb/s QPSK	7 / 25 km	DSP, ADC, DAC,
[15]	A-RoF IFoF	IM/DD	Analog trasceiver	Analog transceiver	-5 dBm	IF: 1.7–2.7 GHz, RF: 28 GHz, 1.5 Gb/s per user, 64-QAM mapped OFDM	20 km	DAC for CA
[16]	A-RoF IFoF	IM+PM / DD	LS, IM+PM, polarization optics	PD + LNA	1 dBm	IF: 14.1 GHz 14×1.2 GHz OFDM CPRI equivalent of 1.032 Tb/s	20 km	IM/PM Tx- for simplified DSP (for CA/CDA)
[17]	A-RoF IFoF	IM/DD	DFB	PD + diff. Balun	-	IF: 0.5, 1.75, and 3 GHz, RF: 60 GHz BW: 305 MHz 16 QAM OFDM, 1 Gb/s	2.2 km	Low
[18]	A-RFoF	Heterodyning 2 tones (LSB+USB)	LS, dual 20 GHz MZM, splitter, oBPF	Fast PD + eBPF + LNA	-8 dBm	Modulation up to 2 Gb/s, DSB RF: 60 GHz (2-tone beating) Alamouti space-time block coding	3 km	Stable LS, eBPF
[19]	A-RoF IFoF Bi-di	IM/DD and coherent heterodyne detection	DML or DFB + MZM	PD+LO Or just PD	HD CRX -16 dBm	IF: 4.7 GHz QPSK, 16-QAM, 64-QAM WDM and FDM	25 km	Virtual tone-based DSP
[20]	D-RoF	IM/DD	64 GS/s DAC 10 GHz DML	10 GHz APD + 80 Gs/s ADC	-8 dBm	10 GHz digitized I/Q data, CW 16 QAM, I/Q 64 QAM	1 km	DSP for CA/DCA + ADC/DAC
[21]	D-RoF FDM	IM/DD	DAC + 2 GHz DML	APD + ADC	-19 dBm	Baseband digitized signals, WDM FDM OFDM	20 km	DSP for CA/CDA, ADC/DAC
[22]	D-RoF IFoF Bi-di	RRH: IM/DD BBU: coh. heterodyne	LS (5 MHz linewidth), IM	10 GHz PIN or het. CRX 90°hybrid	DL: -15 dBm UL: -34 dBm	OFDM at IF: 175, 275 and 375 MHz multi-channel 100/200 Mb/s OOK or 200 Mb/s 16-QAM-OFDM	30 km	ADC and DSP
[23]	A-RoF	Remote heterodyne RH	6 × DFB 6 × MZM AWG MUX	AWG DEMUX LO (DFB) 70 GHz PD 60 GHz amp.	-	RF: 60 GHz 1 Gbit/s OOK	20 km	Stable LO
[24]	A-RoF	DL: IM/DD UL: Coh. heterodyne	DL: dual-drive MZM, UL: EDFA+MZM	DL: APD UL: PIN + DFB as LO	DL: -24 dBm UL: -38 / -34 dBm	1 Gbit/s, DQPSK, SSB and DSB, RF: 1.5, 2.5, 3.5 and 4.5 GHz	12 km	Stable LO
[25]	A-RFoF	Hetero-dyning	DFB, MZM DML (mm-wave) + optical heterodyning	fast PD and LO	-20 dBm mm-wave, -24 dBm WiMAx	400 Mb/s 16 QAM-OFDM Wi-Fi (2.4 GHz), WiMax (5.8 GHz), 1-3 Gbit/s OOK for 60 GHz mm-wave	30 km	Stable LO
[26]	A-RoF IFoF φ-UpC.	Digital coherent 2-tone beating (LSB/USB)	2-tone gen. + AWG 10-20 Gb/s IQ +mod. PDM emulator	PBS+2x UTC-PD +2xOE	-11 dBm	IF: 17.5 GHz 10-20 Gb/s QPSK,	20 km	DSP needed

Abbreviations and symbols used in the table: TX – transmitter, RX – receiver, AWG – arrayed waveguide grating, DML – directly modulated laser, LS – laser source, PD – photodiode, OE – opto-electrical converters, LSB/USB – lower/upper sideband, eBPF/oBPF – electrical/optical bandpass filter, EDFA – Erbium-doped fiber amplifier, CA/CDA – channel aggregation/deaggregation, FDM – frequency division multiplexing, SDM – spatial division multiplexing, DL/UL – downlink/uplink, UTC-PD – uni-traveling-carrier PD, PDM – polarization division multiplexing, WSS – wavelength selective switch, ADC/DAC – analog to digital and digital to analog electrical converters, ECL – external cavity laser, SSB/DSB – single / double sideband, oCS – optical carrier suppression.

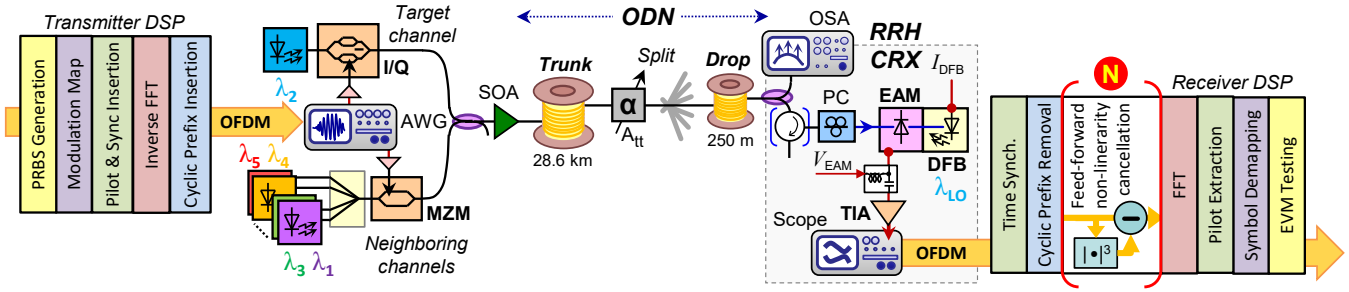

Fig. 3. Experimental setup for coherent homodyne analogue radio-over-fiber transmission and involved DSP stacks at the radio domain.

analog conversion. In its simplest form, A-RoF can be implemented through conveying the native radio signal by means of IM/DD with simple receiver and transmitter elements. However, direct detection is limited in the sensitivity it can obtain. This necessitates optical amplifiers to increase the link budget. Another concern is the spectral efficiency, since the channel spacing in commercial WDM systems resorts to 50 and 100 GHz grids. Coherent detection can offer both, a better sensitivity and a higher spectral efficiency. Technical aspects that remain to be solved are the stability of the LO and the necessity for DSP, rendering these systems as rather challenging to port from the realm of metro-core networks to optical fronthaul applications.

Table I puts into perspective the proposed EML+TIA based receiver with state-of-the-art works on RoF transmission [7-26]. There is an increased interest in A-RoF, with many works targeting transmission through IFoF and RFoF principles, using either IM/DD or coherent detection. The main trade-off between IFoF and RFoF is that IFoF needs additional RF functions such as up/down conversion, whereas the RFoF can save the componentry in this regard in a complexity trade-off with high-bandwidth opto-electronic transceivers. A photonic up-conversion (φ-UpC) is often exploited by beating two independent lasers or two locked tones of a same laser, in order to obtain the desired transfer to the final RF carrier frequency. The requirements on low phase noise using optical heterodyning [25] necessitate narrow laser linewidths. Recent efforts address this challenge through integrated tunable lasers [11] instead of expensive high-performance external cavity lasers.

III. Radio-Transparent Coherent Receiver

The EML is playing a key component role in enabling the simplified homodyne receiver that is transparent to radio signal transmission. First, it includes all required elements such as a laser source as local oscillator (LO) and an absorbing element as photodiode. Second, it contributes to a DSP-free design since synchronized detection is accomplished through all optical locking. Therefore, there is no frequency offset between the signal and the LO and a stable phase between these.

The EML consists of two sections: the electro-absorption modulator (EAM) and the distributed feedback (DFB) laser, both monolithically integrated on a photonic chip. Due to its composite structure it can be used as receiving element as well as transmitting [27]. The EML is foremost known as a transmitter element that is commonly used in fast fiber optical systems [28, 29], where the DFB laser serves as optical signal source and the EAM acts as fast modulator on a basis of the Franz-Keldysh effect [30], where the absorption edge of the device is shifted with the applied bias voltage V_{EAM}. Therefore, when the EAM is used as a modulator – driven with a sufficiently large voltage swing – the output light can be extinguished ($P_O = 0$), leading to a high extinction ratio for the EML transmitter [31]. The transmission transfer function τ of EML is given in [32] as

$$\tau(V_{EAM}) = \frac{P_O(V_{EAM})}{P_{max}(V_{EAM}=0)} = T_0(1-\varepsilon_{min})e^{\left[-\left(\frac{V_{EAM}}{V_a}\right)^{\alpha}\right]} + \varepsilon_{min}, \quad (1)$$

where ε_{min} attributes to the maximum possible extinction, P_{max} is the maximum output optical power when $V_{EAM} = 0$, T_0 resembles the intrinsic losses, and V_a and α are fitting parameters.

When the EML is used as a receiving element, the EAM section takes over the function of a waveguide-structure photodiode. With an appropriate V_{EAM} bias, the level of absorption can be controlled. The higher the reverse bias, the higher is the responsivity of EAM photodiode. The absorbed optical power at the EAM section, which is therefore not visible at the optical output, can be described by a reception function,

$$\rho(V_{EAM}) = 1 - \tau(V_{EAM}) \quad (2)$$

When used as a direct photodetector, the EAM has been proven to have a very high bandwidth [33]. Recently, a -10.9 dBm (BER = 10^{-12}) sensitivity was reached using an EAM-based direct detection receiver at 50 Gb/s [34].

Here, we are aiming at a coherent detection with the EML by virtue of injection locking through the appropriate biasing of its EAM section at semi-transparency, which allows the injection of the optical radio-over-fiber signal P_{RoF} into the DFB (Fig. 2). The injection locking is achieved by temperature- (coarse) or current- (fine) tuning of the DFB emission, in order to allocate it close to the input signal wavelength for stable and precise locking.

The detected EAM photocurrent i_{EAM} of the single-ended coherent receiver is yielded through [35]

This article has been accepted for publication in IEEE/OSA Journal of Lightwave Technology. This is the author's version which has not been fully edited and content may change prior to final publication. Citation information: DOI 10.1109/JLT.2021.3085517

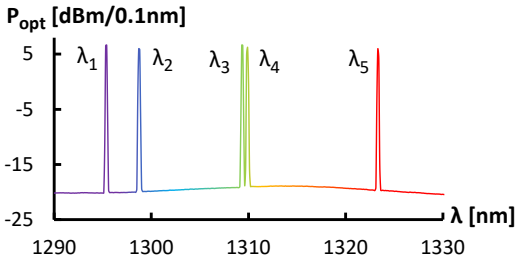

Fig. 4. Transmitted O-band signal spectrum for multi-channel RoF.

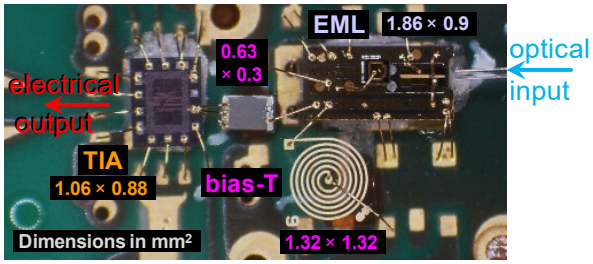

Fig. 5. Receiver assembly with chip-on-carrier EML and die-level TIA.

$$i_{EAM}(t) = R\left[\begin{array}{c} P_{RoF}(t) + P_{LO} + \\ 2\sqrt{P_{RoF}(t)P_{LO}}cos\left(\omega_{IF} + \varphi_{RoF} - \varphi_{LO}\right) \end{array}\right] \quad (3)$$

where R shall be the responsivity of the EAM, P_{LO} is the power of the DFB-based LO, ω_{IF} is the intermediate frequency to which the input signal is down-converted through the coherent detection process, and φ_{RoF} and φ_{LO} are the optical phases of the input signal and the LO, respectively.

There are three terms contributing to the detected photocurrent in this single-ended coherent receiver: First, the direct-detection term that is given through the radio input signal. This term will not be dominant for low received power values. Second, a large dc-term governed by the LO. Third, the coherent beat term between input signal and LO. Since injection locking eliminates the frequency offset, $\omega_{IF} = 0$ and the relative phase between radio-over-fiber signal and LO is constant. With this, the ac-term of the photocurrent for the ideal single-ended receiver, which conveys the information, simplifies to

$$i_{EAM}(t) = 2R\sqrt{P_{RoF}(t)P_{LO}} \quad (4)$$

This relation resembles the detection characteristics of an analogue homodyne receiver and thus obviates the need for frequency offset and carrier-phase compensation via DSP resources, which eventually enables a fully analogue design for the signal converter. The first experimental demonstration of a coherent optical receiver based on an off-the-shelf 10 Gb/s EML butterfly device has been shown in our previous work [4]. Due to the packaged EML device, a built-in isolator at its optical input was contributing to 33.9 dB of optical loss due to its reversed setting. Additionally, due to the 50 Ω interface of the packaged EML, the post-amplification could not be performed via low-noise transimpedance amplifier (TIA), but using a voltage amplifier that increased the system noise and thus decreased the achievable sensitivity.

IV. Experimental Setup

The experimental setup for the characterization of the EML+TIA receiver is depicted in Figure 3. An optical orthogonal frequency division multiplexed (OFDM) signal is generated using an optical inphase/quadrature (I/Q) modulator. The OFDM signal was centered at 3.5 GHz, and it contained 128 sub-carriers within the signal bandwidth of 125 MHz. The OFDM signal had been clipped in order to lower its peak-to-average power ratio. The clipping parameter had been optimized according to the accomplished error vector magnitude (EVM). The I/Q modulator was driven by an arbitrary waveform generator (AWG). We applied optical double-sideband electro-optical modulation at 1298.8 nm. The optical carrier-to-signal power ratio (oCSPR) was set by the I/Q modulator through cancelling out the optical carrier. An O-band semiconductor optical amplifier (SOA) boosted the RoF signal, which was launched with a power of 6 dBm and an optical signal-to-noise ratio of 27.5 dB/0.1 nm. An optical multi-channel feed was created by appending four additional and independently, double-sideband modulated channels at 1295.3, 1309.3, 1309.9, and 1323.3 nm. The launched signal compound is reported in Fig. 4.

We used an ITU-T G.652B-compatible feeder fiber with a length of 28.6 km to emulate the lightpath of the ODN trunk. A variable attenuator (A_{tt}) was used to set the equivalent loss of the distribution split, therefore also determining the optical budget of the ODN. A 250-m long drop fiber completes the connection to the RRH.

At the RRH site, the signal is received through the EML (Fig. 5). The EML was used as a single-polarization and single-ended coherent homodyne detector with co-integrated LO. For the sake of simplicity, the present experiment used a polarization controller (PC) to compensate for the state-of-polarization drift along the fiber-based lightpath. However, polarization-insensitive operation has already been demonstrated through adoption of a diversity receiver scheme [36].

The DSP stacks at the transmitter and receiver, which had been executed off-line, have been included to Fig. 3 and are exclusively serving OFDM modulation and demodulation. No further DSP functions related to coherent optical reception have been performed by virtue of the analogue coherent homodyne receiver.

V. Characterization of the EML+TIA Receiver

In this work, to alleviate the reverse isolation loss that are associated to light injection in packaged EML devices, a chip-on-carrier EML without optical isolator was wire-bonded to the TIA. The corresponding assembly that targets an improved front-end design of the coherent receiver is presented in Fig. 5.

The main challenge, when compared to DD receivers based solely on the EAM photodiode, is the large photocurrent originating from the LO term, as well as a suitable biasing of EAM, TIA, and DFB laser. For this reason, a custom ac-

This article has been accepted for publication in IEEE/OSA Journal of Lightwave Technology. This is the author's version which has not been fully edited and content may change prior to final publication. Citation information: DOI 10.1109/JLT.2021.3085517

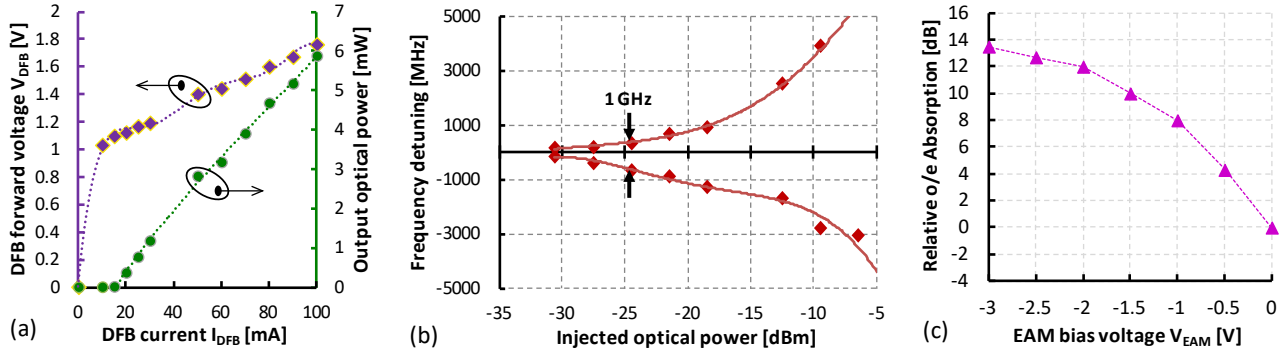

Fig. 6. (a) VLI characteristics of the EML detector. (b) Locking range of the receiver LO. (c) Absorption of the EAM photodiode.

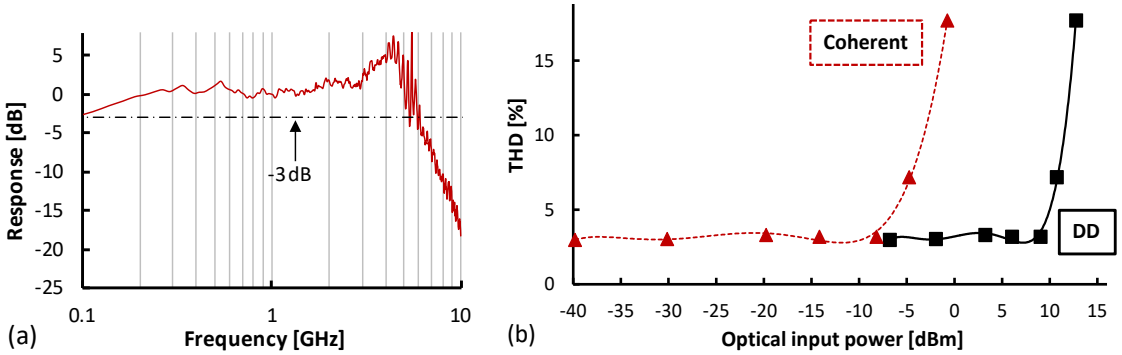

Fig. 7. (a) Opto-electronic response of the TIA under direct detection with the EAM photodiode. (b) THD characteristics of the EML+TIA receiver for direct detection case and coherent detection with an oCSPR of -7 dB and DFB output power of 13.2 dBm.

coupled receiver was implemented with the main trade-off being the added parasitic of decoupling capacitance that can be larger than the EAM parasitic capacitance, thus potentially leading to noise and bandwidth penalties.

A. EML-integrated LO and photodetector

The emission characteristics of the DFB section were characterized in terms of voltage-light-current (VLI). Figure 6(a) shows the VLI for a constant V_{EAM} of –0.8 V. The dependencies can be described by a diode behavior for voltage-to-current conversion (V_{DFB}–I_{DFB}) and an optical output power P_O that increases linearly with laser current I_{DFB} above the threshold I_{th},

$$V_{DFB} = V_J \ln\left(\frac{I_{DFB}}{I_S} + 1\right) + I_{DFB} R_S \quad (5)$$

$$P_O = \eta \frac{hv}{e}(I_{DFB} - I_{th}) \quad (6)$$

where V_J, I_S and R_S are the laser diode junction voltage, saturation current and series resistance, respectively, η is the quantum efficiency, hv is the energy per photon (h is Planck's constant and v is the optical frequency), and e is the elementary charge. From Fig. 6(a), the threshold current is approximately 13 mA; above this value there is a linear L-I relationship. During the transmission experiments, I_{DFB} was set to ~90 mA thus corresponding to the V_{DFB} of 1.7 V. The maximum fiber-coupled power was 7.9 dBm for an I_{DFB} of 100 mA. The spectral characteristics of the DFB-based LO were also evaluated with the optical spectrum analyzer (OSA), showing a side-mode suppression ratio of 50.9 dB. The emission wavelength was 1298.8 nm at a DFB current of 90 mA and a temperature set-point of T = 27°C. Since the photodetection is not being achieved through a balanced detector but instead through the single-ended EML receiver, the relative intensity noise (RIN) of the LO cannot be neglected. The RIN amounted to -157 dB/Hz at the relaxation oscillation peak around 8.2 GHz.

The wavelength locking capabilities of the coherent EML+TIA receiver have been evaluated in terms of locking range [37], which represents the maximal tolerable wavelength detuning, defined as the wavelength mismatch $\Delta\lambda$ between the injected optical signal λ_S and the EML emission wavelength, i.e., its LO wavelength λ_{DFB}. To ensure locking, the mismatch can be minimized through temperature or current tuning of the DFB emission wavelength λ_{DFB}. This can be accomplished at magnitudes of 11.8 GHz/°C and 2.26 GHz/mA for the LO frequency detuning, respectively. During the experiments, temperature and current tuning was performed manually. The locking stability was sufficient for performance evaluation and there was no control applied for the injection locking process. However, a pilot-aided scheme can be adopted for continuous tracking of the locking, as demonstrated in [38].

The locking range is a function of the injected signal power level, and as the injected signal power level decreases so does the locking range, meaning that λ_S and λ_{DFB} cannot be significantly spectrally displaced for a low optical input power. The injected unmodulated optical signal was kept at a fixed value of λ_S = 1298.865 nm and its injected optical power was adjusted through a variable attenuator in the range from -3.5 dBm down to –30.6 dBm. Figure 6(b) reports the locking range for an EAM photodiode bias of –0.75 V. At a low input

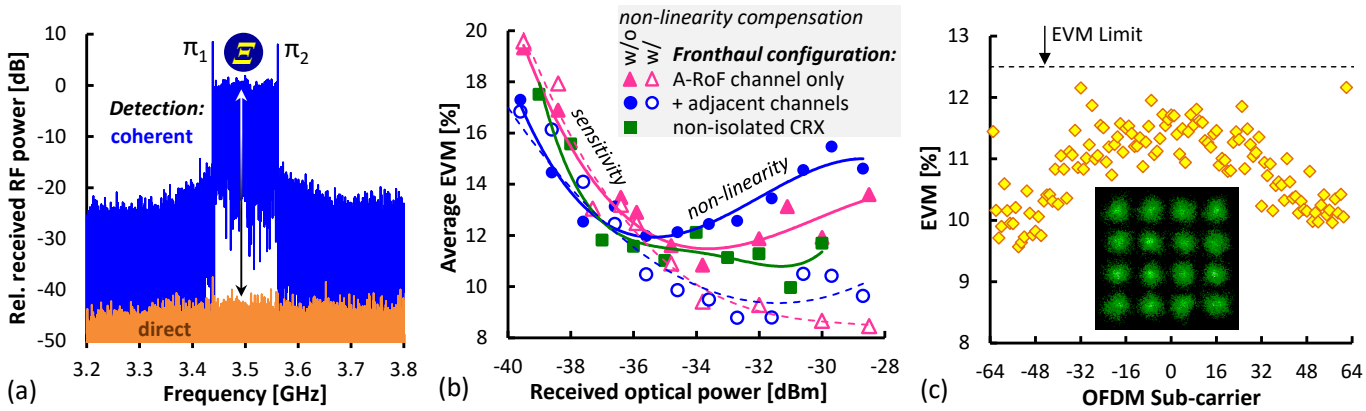

Fig. 8. (a) Received OFDM spectrum after coherent homodyne detection. (b) EVM as function of the received power and (c) sub-carrier index.

signal power of –30.6 dBm, the locking range is 160 MHz. It increases to 5.7 GHz for a high input of –3.5 dBm. These values – even at the lowest input power – are enough to absorb typical wavelength drifts of laser source due to a sub-optimal thermo-electric control. In our previous studies [4, 39], building on C-band butterfly and TO-can EMLs, similar values of 200 and 215 MHz were obtained for the locking range at an input of –27.8 and –30 dBm, respectively.

The absorption characteristics of the EAM section were obtained by applying an external optical input with a 1 GHz tone and observing its magnitude at the output. Figure 6(c) presents the bias-dependent absorption characteristics relative to V_{EAM} = 0V. The difference between the unbiased case (V_{EAM} = 0) and a fully reversed bias (V_{EAM} = –3 V) was ~14 dB. A steep rise for low bias magnitudes enables photodetection at a semi-transparent EAM section, which contributes to a wider locking range.

B. *EML+TIA receiver assembly*

The used chip-on-carrier EML, shown in Fig. 5, is rated for wavelength-stacked local area network (LAN-WDM) applications at 28 Gb/s transmission. Its emission in the O-band region is 1295.56 nm at room temperature. The choice of the O-band for A-RoF transmission is solely based on the availability of EML devices.

The photocurrent generated within the EAM is amplified and converted to a voltage signal by the TIA. Both components, EML and TIA, are used in die form to avoid the package parasitic and to insure the stability of the circuit. The –3-dB bandwidth of the TIA is rated at 9 GHz for the photodetector capacitance of 220 fF. The measured TIA bandwidth of 6.1 GHz (Fig. 7(a)) is smaller than this due to the additional parasitic components of the ac-coupling capacitor. Since the EAM photocurrent consists of the large dc component of the DFB-based LO, EML and TIA were ac-coupled using a bondable 10 nF capacitor, whereas the dc current was steered away from the TIA through a bondable inductor. Due to the relatively low inductance and relatively large Q-factor of this bondable inductor, a wideband discrete bias-T was additionally used in the EAM bias branch.

The receiver linearity was investigated via total harmonic distortion (THD) measurements for a sinusoidal input signal. For this purpose, a 1299 nm source was modulated via Mach-Zehnder modulator (MZM) with a 1 GHz sine wave. The linearity of this transmitter test-set was verified with broadband PIN photodiode, showing a THD of 0.7%.

For the DD case with the EML+TIA subassembly, the input power was varied in the range from -6.8 dBm to 12.75 dBm and the obtained THD was 3% in average, up to 9 dBm. For the coherent reception case, the maximum permissible input range would be shifted to lower input power values due to the beating with the LO and the possibility to suppress the optical carrier. Assuming that the same TIA current i_{TIA} leads to the same THD, the sensitivity of the coherent reception case to THD relates to that of the DD case according to

$$i_{TIA} = RP_{DD} = 2R\sqrt{P_{coh}\, oCSPR\, P_{LO}} \tag{7}$$

where P_{DD} and P_{coh} are the optical input power levels, respectively. Their interrelation is then yielded through

$$P_{coh} = \frac{P_{DD}^2}{4\, oCSPR\, P_{LO}} \tag{8}$$

For example, at oCSPR of -7 dB and at a DFB power of 13.2 dBm (estimated from the EAM current and a supposed responsivity of 1 A/W, respectively) the maxim input optical power range would be limited up to –8.2 dBm for a THD of 3%. If the responsivity is very low, for example 0.1 A/W, then for the same operating conditions (I_{EAM} = 21 mA) the corresponding LO power of 23.22 dBm leads to the maximum input signal of –18.2 dBm for a THD of 3%. Therefore, even for high LO power values, there is a wide range for the input signal power for which the THD value is approximately 3%, which should give receiver sensitivity degradation below 1 dB for 16-QAM signals [40]. Both the measured (DD) and estimated THD curve are shown in Fig. 7(b) for a coherent-reception LO power of 13.22 dBm.

VI. Radio Transmission Performance

The transmission performance was evaluated through the EVM values for sub-carriers of OFDM signal containing quadrature phase shift keying (QPSK) and 16-point quadrature

amplitude modulation (QAM) formats. The oCSPR was chosen with -7 dB. This value corresponds to a highly suppressed optical carrier, since its main purpose is to achieve receiver locking, which is possible for low optical injection levels [4, 37]. Figure 8(a) shows the signal spectra received at the RRH for both cases – coherent detection, where the DFB section of the EML served as a local oscillator, and direct detection with dark LO. At a received optical power in the range of –35 dBm, the clearance Ξ between coherent and direct detection terms is more than 40 dB since there are no direct-detection components above the noise floor. Moreover, the two pilots (π_1,π_2) at the spectral border of the OFDM signal are clearly distinguishable in the RF domain, evidencing that the EML+TIA receiver accomplishes coherent homodyne detection with good signal integrity.

Figure 8(b) reports the EVM performance for the receiver that is isolated from optical feedback at the drop segment, in case of single- (λ_2,▲), and multi-channel transmission (λ_1…λ_5,●). In case of single-channel transmission at the wavelength λ_2 (▲), the EVM was below the 12.5% antenna limit for received optical power levels above –36.1 dBm. Considering the transmitted signal launch, this resembles an optical budget of 42.1 dB, which is large enough to absorb both, the O-band feeder fiber transmission loss and a 1:128 splitting loss. Taking into account contribution of these basic losses, a large power margin of 12.8 dB is obtained. Signal reception is limited by two factors. The first is the noise limit for lower received power levels, whereas the second is the non-linearity imposed by the saturation of the receiver for higher received power levels, larger than –32 dBm. This power level is below the region of rising THD (Fig. 7(b)). It nevertheless limits the dynamic range that is supported by the receiver and therefore requires further improvement – although the source of signal distortion could not be precisely elucidated. An incorrect optical transmitter setting was ruled out by means of an optical back-to-back measurement using a direct-detection PIN receiver at the I/Q modulator output, yielding a low EVM of 4.7%.

Figure 8(c) presents the EVM for all OFDM sub-carriers at a received power of –34 dBm, which marks the onset of non-linearity. The inset shows the compound constellation diagram of a received 16QAM-OFDM signal.

In order to elaborate on the EVM performance without non-linear penalty, the DSP stack at the receiver has been modified. A beat interference estimation and cancellation, similar as in [41], has been included in the receiver-side DSP stack between time synchronization and OFDM demodulation (N in Fig. 3) and its feed-forward parameters have been chosen off-line to optimize the reception. An EVM improvement of 5.1% at the input optical power of –28.5 dBm is possible if the DSP-assisted non-linear mitigation is used (△), leading to an EVM below the 64-QAM antenna limit.

After the inclusion of four co-propagating adjacent channels, there is no penalty at optical power levels towards the noise limit (●), but the performance decreases towards higher received power values. The rise of EVM occurs earlier, at a ~2.5-dB lower power level for the received signal. The reason for this penalty is the single-ended input of the optical receiver, which therefore does not have a common-mode rejection capability. As for the single-channel scenario, the non-linear EVM penalty can be compensated through additional DSP functions (○), indicating the potential for low EVM values for a linearized receiver.

We have further emulated a more realistic deployment scenario, in which the coherent receiver is not isolated but directly connected to the corresponding fiber of the drop span, which exposes it to various optical feedback effects for high optical budgets. This scenario was investigated for the single-channel performance, where the optical circulator before the EML+TIA receiver was removed (■). We did not observe a penalty compared to the optically isolated case.

VII. Conclusion

We have demonstrated a simple EML+TIA coherent homodyne receiver in an A-RoF application scenario that is capable of operating in a DSP-free fashion. This is the first time that an EML is co-integrated to a TIA circuit and used as a coherent receiver. The receiver accomplishes a high reception sensitivity of –36 dBm for a single-carrier, 125-MHz wide OFDM signal modulated at a carrier at 3.5 GHz. This sensitivity enables high optical budget of 42.1 dB, thus allowing for a 1:128 splitting loss besides a fiber reach of 28.8 km. The filterless reception in presence of four adjacent RoF channels has been experimentally confirmed. The main drawbacks of the current receiver are relatively high EVM values, which do not leave much margin for wireless signal transmission. Possible reasons for these high EVM values could lie in the sensitive interface between TIA and its bias-T, giving rise to peaking behavior in transfer function and even reflections. Future work will aim to improve the receiver design by choosing different components to realize an improved biasing branch as well as sensitivity to input capacitance. Additionally, a balanced receiver architecture can serve the rejection of laser and adjacent channel noise, while linearity is to be improved in order to extend the dynamic range of the proposed low-complexity coherent receiver.

References

[1] M. Shafi *et al.*, "5G: A tutorial overview of standards, trials, challenges, deployment, and practice," *IEEE J. Sel. Areas Commun.*, vol. 35, no. 6, pp. 1201-1221, Jun. 2017.

[2] K. Sakaguchi *et al.*, "Where, When, and How mmWave is Used in 5G and Beyond," *IEICE Trans. on Electron.*, vol. 100, no. 10, pp. 790-808, Oct. 2017.

[3] J. Yao, "Microwave Photonics," *IEEE/OSA J. Lightwave Technol.*, vol. 27, no. 3, pp. 314-335, Feb. 2009.

[4] B. Schrenk, "Injection-Locked Coherent Reception Through an Externally Modulated Laser," *IEEE J. Sel. Top. Quantum Electron.*, vol. 24, no. 2, p. 3900207, Mar. 2018.

[5] D. Milovancev, N. Vokic, F. Karinou, and B. Schrenk, "Simplified Coherent Receiver for Zero-Touch Wireless Integration in Power-Splitting ODN with >40 dB Budget," in *Proc. Opt. Fiber Comm. Conf.*, San Francisco, United States, Jun. 2021, accepted for publication

[6] A. Udalcovs *et al.*, "Total Cost of Ownership of Digital vs. Analog Radio-Over-Fiber Architectures for 5G Fronthauling," *IEEE Access*, vol. 8, pp. 223562-223573, Dec. 2020.

[7] X. Liu, H. Zeng, N. Chand, and F. Effenberger, "Efficient Mobile Fronthaul via DSP-Based Channel Aggregation," *IEEE/OSA J. Lightwave Technol.*, vol. 34, no. 6, pp. 1556-1564, Mar. 2016.

[8] H.N. Parajuli, H. Shams, L. Guerrero Gonzalez, E. Udvary, C. Renaud, and J. Mitchell, "Experimental demonstration of multi-Gbps multi sub-bands FBMC transmission in mm-wave radio over a fiber system," *OSA Opt. Expr.*, vol. 26, no. 6, pp.7306-7312, Mar. 2018.

[9] M. Sung *et al.*, "RoF-based radio access network for 5G mobile communication systems in 28 GHz millimeter-wave," *IEEE/OSA J. Lightwave Technol.*, vol. 38, no. 2, pp. 409-420, Jan. 2020.

[10] E. Ruggeri *et al.*, "Multi-user IFoF uplink transmission over a 32-element 60GHz phased array antenna enabling both frequency and spatial division multiplexing," in *Proc. Europ. Conf. Opt. Comm.*, Dublin, Ireland, Sep. 2019, paper M.2.C.5.

[11] C. Browning, A. Delmade, Y. Lin, D. H. Geuzebroek, and L. P. Barry, "Optical Heterodyne Millimeter-Wave Analog Radio-Over-Fiber with Photonic Integrated Tunable Lasers," in *Proc. Opt. Fiber Comm. Conf.*, San Diego, United States, Mar. 2019, paper W1I.4.

[12] D. Perez-Galacho, D. Sartiano, and S. Sales, "Analog Radio over Fiber Links for Future 5G Radio Access Networks," in *Proc. 21st Int. Conf. Transparent Opt. Netw.*, Angers, France, Jul. 2019, paper Fr.B1.2.

[13] D. Konstantinou, A. Morales, S. Rommel, T. R. Raddo, U. Johannsen, and I. T. Monroy, "Analog Radio Over Fiber Fronthaul for High Bandwidth 5G Millimeter-Wave Carrier Aggregated OFDM," in *Proc. 21st Int. Conf. Transparent Opt. Netw.*, Angers, France, Jul. 2019, paper Th.B2.3.

[14] G. Giannoulis *et al.*, "Analog Radio-over-Fiber Solutions for 5G Communications in the Beyond-CPRI Era," in *Proc. 20th Int. Conf. Transparent Opt. Netw.*, Bucharest, Romania, Jul. 2018, paper Mo.B2.6.

[15] M. Sung, S. Cho, J. Kim, J. K. Lee, J. H. Lee, and H. S. Chung, "Demonstration of IFoF-based mobile fronthaul in 5G prototype with 28-GHz millimeter wave," *IEEE/OSA J. Lightwave Technol.*, vol. 36, no. 2, pp. 601-609, Jan. 2018.

[16] S. Ishimura, A. Bekkali, K. Tanaka, K. Nishimura, and M. Suzuki, "1.032- Tb/s CPRI-equivalent rate IF-over-fiber transmission using a parallel IM/PM transmitter for high-capacity mobile fronthaul links," *IEEE/OSA J. Lightwave Technol.*, vol. 36, no. 8, pp. 1478-1484, Apr. 2018.

[17] U. Habib, M. Steeg, A. Stoehr, and N. Gomes, "Radio-over-fiber-supported 60 GHz multiuser transmission using leaky wave antenna," in *Proc. IEEE Int. Topical Meeting Microw. Photon.*, Beijing, China, Oct. 2017, paper Th2.3.

[18] Y. Tian, K. L. Lee, C. Lim, and A. Nirmalathas, "Performance evaluation of CoMP for downlink 60-GHz radio-over-fiber fronthaul," in *Proc. IEEE Int. Topical Meeting Microw. Photon.*, Beijing, China, Oct. 2017, paper Tu3.2.

[19] M. Xu *et al.*, "Bidirectional fiber-wireless access technology for 5Gmobile spectral aggregation and cell densification," *IEEE/OSA J. Opt. Commun. Netw.*, vol. 8, no. 12, pp. 104-110, Dec. 2016.

[20] X. Liu, H. Zeng, N. Chand, and F. Effenberger, "CPRI-compatible efficient mobile fronthaul transmission via equalized TDMA achieving 256 Gb/s CPRI-equivalent data rate in a single 10-GHz-bandwidth IM-DD channel," in *Proc. Opt. Fiber Comm. Conf.*, Anaheim, United States, Mar. 2016, paper W1H.3.

[21] F. Effenberger, and X. Liu, "Power-efficient method for IM-DD optical transmission of multiple OFDM signals," *OSA Opt. Expr.*, vol. 23, no. 10, pp. 13571-13579, May 2015.

[22] M. Zhu, F. Li, F. Lu, J. Yu, C. Su, G. Gu, and G.-K. Chang, "Wavelength resource sharing in bidirectional optical mobile fronthaul," *IEEE/OSA J. Lightwave Technol.*, vol. 33, no. 15, pp. 3182-3188, Aug. 2015.

[23] M.P. Thakur, S. Mikroulis, C.C. Renaud, J.E. Mitchell, A. Stoehr, "DWDM-PON/mm-wave wireless converged next generation access topology using coherent heterodyne detection", in *Proc. 16th Int. Conf. Transparent Opt. Netw.*, Graz, Austria, Jul. 2014, paper Tu.D4.2.

[24] C. Kottke, K. Habel, M. H. Eiselt, H. Griesser, and J. P. Elbers, "Coherent subcarrier-WDM-PON system with SSB modulation and wavelength reuse," in *Proc. Opt. Fiber Comm. Conf.*, Anaheim, United States, Mar. 2013, paper OM2A.3.

[25] C. Liu, L. Zhang, M. Zhu, J. Wang, L. Cheng, and G. Chang, "A Novel Multi-Service Small-Cell Cloud Radio Access Network for Mobile Backhaul and Computing Based on Radio-Over-Fiber Technologies," *IEEE/OSA J. Lightwave Technol.*, vol. 31, no. 17, pp. 2869-2875, Sept. 2013.

[26] A. Kanno *et al.*, "Optical and millimeter-wave radio seamless MIMO transmission based on a radio over fiber technology," *OSA Opt. Expr.*, vol. 20, no. 28, pp. 29395-29403, Dec. 2012.

[27] B. Schrenk, "The Electroabsorption-Modulated Laser as Optical Transmitter and Receiver: Status and Opportunities", *IET Optoel.*, vol. 14, no. 6, pp. 374-385, Dec. 2020.

[28] O. Ozolins *et al.*, "100 GHz Externally Modulated Laser for Optical Interconnects," *IEEE/OSA J. Lightwave Technol.*, vol. 35, no. 6, pp. 1174-1179, Mar. 2017.

[29] R. Lewen, S. Irmscher, U. Westergren, L. Thylen, and U. Eriksson, "Segmented Transmission-Line Electroabsorption Modulators," *IEEE/OSA J. Lightwave Technol.*, vol. 22, no. 1, pp. 172-179, Jan. 2004.

[30] G. L. Li, and P. K. L. Yu, "Optical Intensity Modulators for Digital and Analog Applications", *IEEE/OSA J. Lightwave Technol.*, vol. 21, no. 9, pp. 2010-2030, Sep. 2003.

[31] H. Dalir, Y. Takahashi, and F. Koyama, "Low driving voltage (<400 mVpp) electro-absorption modulator laterally integrated with VCSEL", in *Proc. Opt. Fiber Comm. Conf.*, San Francisco, United States, Mar. 2014, paper W4C.3.

[32] R. A. Salvatore, R. T. Sahara, M. A. Bock and I. Libenzon, "Electroabsorption modulated laser for long transmission spans," *IEEE J. of Quantum Electron.*, vol. 38, no. 5, pp. 464-476, May 2002.

[33] M. Chacinski, U. Westergren, L. Thylen, R. Schatz, and B. Stoltz, "50 Gb/s Modulation and/or Detection with a Travelling-Wave Electro-Absorption Transceiver," in *Proc. Opt. Fiber Comm. Conf.*, San Diego, United States, Feb. 2008, paper JThA32.

[34] M. Raj *et al.*, "Design of a 50-Gb/s Hybrid Integrated Si-Photonic Optical Link in 16-nm FinFET," *IEEE J. Solid-State Circ.*, vol. 55, no. 4, pp. 1086-1095, Apr. 2020.

[35] K. Kikuchi, "Fundamentals of Coherent Optical Fiber Communications," *IEEE/OSA J. Lightwave Technol.*, vol. 34, no. 1, pp. 157-179, Jan. 2016.

[36] B. Schrenk, and F.Karinou, "Simple Laser Transmitter Pair as Polarization-Independent Coherent Homodyne Detector," *OSA Opt. Expr.*, vol. 27, no. 19, pp. 13942-13950, May 2019.

[37] R. Hui, A. D'Ottavi, A. Mecozzi, and P. Spano, "Injection Locking in Distributed Feedback Semiconductor Lasers," *IEEE J. Quantum Electron.*, vol. 27, no. 6, pp. 1688-1695, Jun. 1991.

[38] Z. Liu, J. Kim, D. S. Wu, D. J. Richardson, and R. Slavik, "Homodyne OFDM with Optical Injection Locking for Carrier Recovery," *IEEE/OSA J. Lightwave Technol.*, vol. 33, no. 1, pp. 34-41, Jan 2015.

[39] B. Schrenk, and F. Karinou, "A Coherent Homodyne TO-Can Transceiver as Simple as an EML", *IEEE/OSA J. Lightwave Technol.*, vol. 37, no. 2, pp. 555-561, Jan. 2019.

[40] M. G. Ahmed, T. N. Huynh, C. Williams, Y. Wang, P. K. Hanumolu, and A. Rylyakov, "34-GBd Linear Transimpedance Amplifier for 200-Gb/s DP-16-QAM Optical Coherent Receivers," *IEEE J. Solid-State Circ.*, vol. 54, no. 3, pp. 834-844, Mar. 2019.

[41] W.R. Peng *et al.*, "Spectrally efficient direct-detected OFDM transmission employing an iterative estimation and cancellation technique," *OSA Opt. Expr.*, vol. 17, no. 11, pp. 9099-9111, 2009.